34th Annual International Conference of the IEEE EMBS
San Diego, California USA, 28 August - 1 September, 2012

Patch-based Automatic Retinal Vessel Segmentation in Global and Local Structural Context

Shuoying Cao*, Anil A. Bharath, Kim H. Parker and Jeffrey Ng

Abstract— **In this paper, we extend our published work [1] and propose an automated system to segment retinal vessel bed in digital fundus images with enough adaptability to analyze images from fluorescein angiography. This approach takes into account both the global and local context and enables both vessel segmentation and microvascular centreline extraction. These tools should allow researchers and clinicians to estimate and assess vessel diameter, capillary blood volume and microvascular topology for early stage disease detection, monitoring and treatment. Global vessel bed segmentation is achieved by combining phase-invariant orientation fields with neighbourhood pixel intensities in a patch-based feature vector for supervised learning. This approach is evaluated against benchmarks on the DRIVE database [2]. Local microvascular centrelines within Regions-of-Interest (ROIs) are segmented by linking the phase-invariant orientation measures with phase-selective local structure features. Our global and local structural segmentation can be used to assess both pathological structural alterations and microemboli occurrence in non-invasive clinical settings in a longitudinal study.**

I. INTRODUCTION

Attempts to study the retinal vascular system date back to the origins of ophthalmoscopy in the 19th century. This is partly because the microvascular blood flow can be visually inspected non-invasively, offering a unique opportunity to study human haemodynamics by examining the ocular circulation. Over the years, clinical and research assessment techniques have evolved from the physical description of selected retinal arteries and veins to the quantitative measurements of the associated ocular haemodynamic parameters [3]. These quantitative parameters, describing the characteristics of retinal vasculature or ocular blood perfusion, can be influenced by the presence of diseases such as hypertension [4], diabetes [5] and glaucoma [6]. Any attempt to automate the measurements of these characteristics relies on an accurate system to segment the retinal vasculature automatically. Over the years, various methods [7] for retinal vessel segmentation have been proposed and benchmarked on shared image repositories. One of such publicly available databases is "DRIVE" (Digital Retinal Images for Vessel Extraction) [2]. This database contains images directly acquired from a digital fundus camera and also contains manual segmentation by different observers. This captures some of the variability found in manual segmentation.

Our paper is organized as follows. In Section II, we introduce our automated segmentation method. We first construct, in Section II-A, a phase-invariant orientation field using steerable wavelet filters that can be used to help differentiate the vessels from background. In Section II-B, phase-invariant structural information is combined with neighbourhood pixel intensities to segment the global retinal vessel bed. In Section II-C, we combine these phase-invariant features with pixelwise phase-selective responses to identify and extract the local microvascular centreline. In Section III, we present the comparison of our vessel segmentation algorithm with other benchmark algorithms.

*S. Cao, A. A. Bharath, K. H. Parker and J. Ng are with Bioengineering Department, Imperial College London, South Kensington Campus, London SW7 2AZ (email: shuoying.cao@imperial.ac.uk).

II. SEGMENTATION

Extensive research on vessel segmentation has been published. Methods include: Laplacian-of-Gaussian filtering with binary image morphology [8]; two-dimensional Gaussian models of vessel intensity space [9]; exploratory vessel tracing [10], region-growing using Hessian matrix maxima in Gaussian scale-space [11] and maximum likelihood estimates from multi-scale Gaussian filter outputs [12]. With retinal arterioles typically ranging from approximately 20 to 200μm in diameter [13], the microvascular structures in the scale of 10μm are often visualized by fluorescein angiography alone. Meanwhile, funduscopy is popular in national eye screening programmes for diabetic retinopathy. Yet, most algorithms are developed on either red-free fundus images or fluorescein angiograms. Thus, there is a need for techniques that take into account this scale difference between the two image modalities, yet employ some parameters that are unique and distinctive enough to classify both the entire vessel bed (red-free) and the micro-vessel (fluorescein) centrelines.

A. Phase-invariant Orientation Field

The feature that we use is defined in prior works [14], [15] and [16]. Because red-free and fluorescein images have opposite contrast behavior, this approach compactly encodes the neighbourhood phase-invariant structural orientation and spatial symmetry estimate. It also shares some benefits of the scale-space approach as the filter scale selection is automated to be "scalable" to the local vessel diameter. This tuning takes the form of a weighting applied to each scale of the filter output, based on the likelihood of that filter scale being well matched to the local vessel size. In-depth discussion and application of "steering in scale" and "detecting intrinsic scale" in a more generalized setting can be found in [16].

The phase-invariant orientation field is a representation of local image structure that is relatively discriminating, yet stable in the presence of illumination change. It may be thought of as a quasi-illumination invariant estimation of local structure orientation, independent of local spatial symmetry about a selected dominant axis (see Figure 1).

978-1-4577-1787-1/12/$26.00 ©2012 IEEE

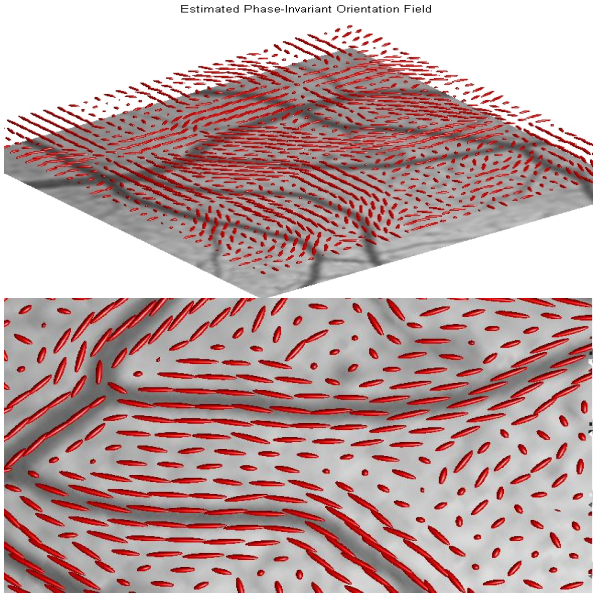

Fig. 1. *Estimated phase-invariant orientation field (in red) of a* 128×128 *patch from a retinal fluorescein angiogram with 3D view (top) and detailed 2D view (bottom).*

It is constructed as:

$$\overrightarrow{\mathrm{O}}^{(l)}(x,y) = \frac{\sum_{k=0}^{K/2-1} |g_k^{(l)}(x,y)| \vec{u}_k}{p + (\sum_{k=0}^{K/2-1} |g_k^{(l)}(x,y)|^2)^{\frac{1}{2}}} \tag{1}$$

for $g_k^{(l)}(x,y)$ where $k = 0,1,2,...,\frac{K}{2}$-1 denotes the output of the k^{th} oriented bandpass complex analysis filter from image f at level l. For $K = 8$, we use four direction vectors $\vec{u} = \{[1,0],[0,1],[\text{-}1,0],[0,\text{-}1]\}$. Note the *double-angle* nature of these direction vectors relative to the *single-angle* directional filter kernels (see Figure 2).

p is a conditioning constant set at 1.25% of the maximum value of the image [15]. As the magnitude of the phase-invariant orientation field $\overrightarrow{\mathrm{O}}^{(l)}(x,y)$ ranges from 0 to 1, it can be used as an indication of anisotropy, in which strongly isotropic neighbors will produce values near to 0 and strongly anisotropic neighbors will produce values near to 1.

Our set of four 15 × 15 complex "Steerable Wavelet Filter" (SWF) arrays can be visualized in Figure 2.

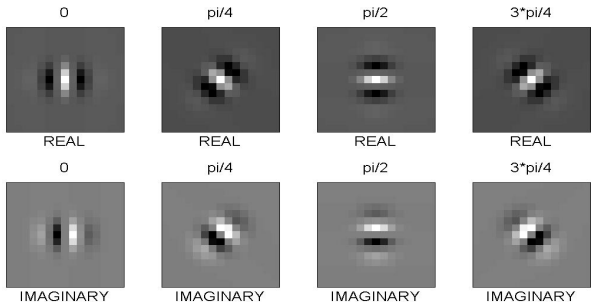

Fig. 2. *Real and imaginary parts of oriented complex bandpass filter kernels used to produce the filter outputs in the spatial domain.*

B. Vessel Segmentation

Niemeijer [2] proposed a supervised pixel classification method such that for each pixel in the image, a 31-dimensional feature vector is constructed and a kNN-classifier is trained with these feature vectors. Their study also showed that the kNN-classifier performed better than a linear or a quadratic classifier. This architecture first appeared as *convolutional neural nets* [17] used for recognizing handwritten characters. We suggest instead a smaller feature vector that relies on the phase-invariant orientation field over a local patch, combined with pixel intensities over the patch. A standard artificial neural network [18] is then trained over a small sample of labeled pixels to effect the segmentation. We use a multi-layer feed-forward network with backpropagation and the Levenberg-Marquardt training algorithm [19]. The network uses a scaled conjugate gradient descent training function, a mean squared error performance function, and hyperbolic tangent sigmoid transfer functions for both hidden and output layers. Our 27-dimensional input feature vector is defined as [20]:

$$\overrightarrow{\mathrm{FV}} = [\mathrm{I}_{3\times3}, \overrightarrow{\mathrm{O}}_{(3\times3)}] \tag{2}$$

Our unique descriptors for segmentation is assembled as follows: For each pixel, we first assemble its 3×3 neighbourhood intensity. We then separate the horizontal and vertical components of the orientation field vectors, and assemble the $2 \times 3 \times 3$ structural orientation matrix. Note, the horizontal and vertical components of the orientation vectors are normalized as a pair against 2D vector magnitudes to conserve the angular representation at each location in the neighbourhood. For training, we use randomly selected patches (similar to a discretized Wiener process) from each training image and validate the accuracy of the classification output against manually segmented ground-truth from the DRIVE database.

C. Centreline Extraction

Methods for line detection, tracing and extraction include active contours [21], the Hough transform [22] and scale-space filters (Principal Component Analysis of the Hessian matrix) combined with region growing [11]. To achieve subpixel accuracy in centreline positions, Steger [23] used the Gaussian partial derivative kernels to characterize the first and second directional derivative of curvilinear structures. To detect regions of high directional curvature, the scale of the applied Gaussian kernels is vital for accuracy. If the standard deviation of the Gaussian kernel is too small, the vessel centrelines cannot be detected.

We use a "link while extract" piece-wise segmentation approach that combines the search algorithm with our phase-invariant orientation field, improving on Steger's method [23] that only links "selected" vessel centerline pixels *after* extraction. In a neighbourhood $\Theta(p,r)$ from image f, the pixel $p = (p_x, p_y)$ locates at the centre of the $r \times r$ patch. Now if, for instance, the local vascular (neighbourhood) orientation $\overrightarrow{\mathrm{O}}_{\Theta}^{(l)}((x,y) \in \Theta)$ at scale l is in the interval $[-\frac{\pi}{8}, \frac{\pi}{8}]$, then only the points (p_x+1, p_y+1), (p_x+1, p_y), (p_x+1, p_y-1) are considered as "locally aligned" pixels.

Meanwhile, we use an additional measure that estimates local phase for each pixel. This estimate, $\Psi^{(l)}$, is obtained from the complex wavelet filter outputs steering by the polynomial functions $s_p(\phi,k)$ and $s_q(\phi,k)$ on image f [15]. For ϕ being the angle indicating the direction of $\overrightarrow{\mathrm{O}}^{(l)}(x,y)$:

$$\Psi^{(l)} = \angle \left(\sum_{k=0}^{K/2-1} s_p(\phi,k) g_k^{(l)}(x,y) + \sum_{k=0}^{K/2-1} s_q(\phi,k) (g_k^{(l)}(x,y))^* \right) \quad (3)$$

p is considered as a "probable" vessel centreline pixel if its local phase estimate, $\Psi^{(l)}(p_x, p_y)$, matches the phase component of its neighbourhood $\overrightarrow{O}_{\Theta}^{(l)}$. The angular difference between p and its "locally aligned" pixels determines whether these neighboring pixels are also likely to be located along the vessel centreline. The combination of both allows a soft classification of the centreline (sub)pixel locations. The Euclidean distance between two neighbouring (sub)pixels is also calculated as an indicator for the continuity of the vessel.

III. Experiments and Results

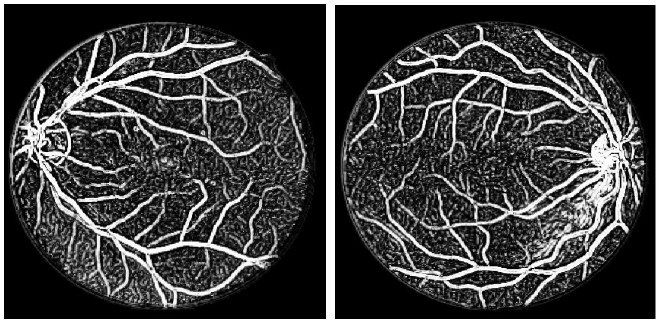

Fig. 3. *The posterior probability map ("soft decision") of our SWF-NN segmentation result using test image 1 (left) and test image 20 (right).*

To compare our automatic vessel segmentation technique with several (8) previously benchmarked methods [7][2][8][24][11][9][25], we tested our algorithms on the DRIVE database and adopted the same evaluation protocol: as suggested in [2], the performance of all algorithms was only evaluated on the test image set to prevent bias between supervised and unsupervised vessel segmentation methods.

Figure 3 shows the segmentation results of the global vessel-bed of two test images. The photographs for the DRIVE database were obtained from a diabetic retinopathy screening program in The Netherlands. The 40 images were acquired using a Canon CR5 non-mydriatic 3CCD camera with a 45 degree field of view (FOV). Each image was captured using 8 bits per color plane at 768 by 584 pixels. The FOV of each image is circular with a diameter of approximately 540 pixels. The set of 40 images has been divided into a training and a test set, each with 20 images.

For training, we generated 5 different batches of random patch from each training image: 4000 pixels (0.89% of total image pixels), 8000 pixels (1.78%), 12000 pixels (2.68%), 16000 pixels (3.57%) and 24000 pixels (5.35%). Each patch contains approximately equal numbers of vessel and background pixels. We compared network models constructed from training based on 8×10^4 pixels, 1.6×10^5 pixels, 2.4×10^5 pixels, 3.2×10^5 pixels and 4.8×10^5 pixels.

Figure 4 (top) presents a classic ROC curve across the entire test image set using our algorithm. Figure 4 (bottom) demonstrates the algorithm performance from eight different benchmark methods. Single points on the figure represent binary segmentation methods. Table I compares the area under the ROC curve (A_z) for non-binary segmentation

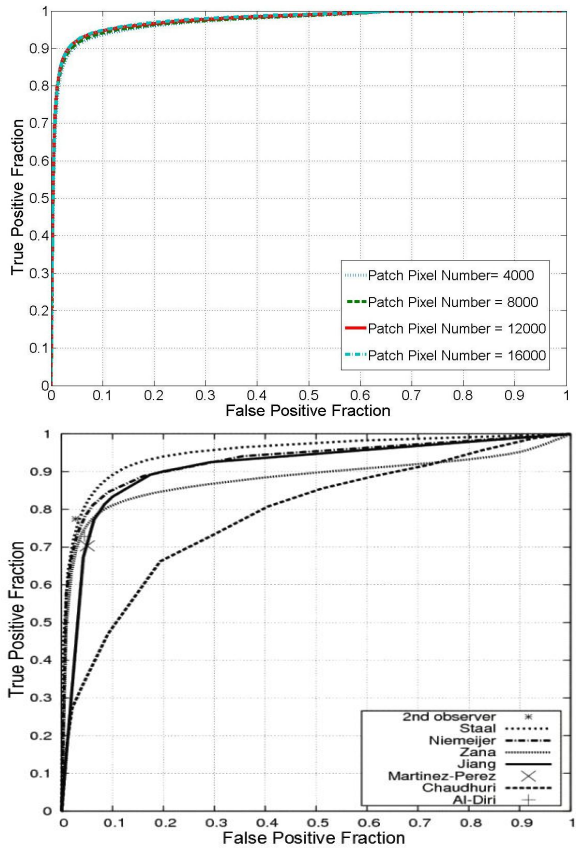

Fig. 4. *Top: The ROC curves of our SWF-NN algorithm evaluated on the DRIVE database with different training patch size, incrementing from less than 1% to around 5% of the total image pixels; Bottom: The ROC curves of 8 methods tested on the DRIVE database, adapted from [7].*

methods. Our "Steerable Wavelet Filter-Neural Network" (SWF-NN) algorithm achieved 0.9779 for A_z.

Method	**SWF-NN**	**Staal**	**Martinez-Perez**	**Niemeijer**
A_z	**0.98**	0.95	0.93	0.93
Method	**Jiang**	**Zana**	**Chaudhuri**	**Human Observer**
A_z	0.91	0.90	0.79	n/a

TABLE I

A_z COMPARISON FOR 8 SEGMENTATION METHODS

Since poor performance on a single image may be masked in an ROC curve for an image set, we applied the same neural network model on each of the 20 test images in the DRIVE database individually. The ROC for the entire test data superimposed on the ROC lower and upper bounds (per image) is depicted in Figure 5.

The results for microvascular centreline segmentation on sequential fluorescein angiograms were presented and discussed in depth in our previous publication [1].

IV. Conclusion

In this paper, we suggest a patch-based structural approach for retinal vasculature segmentation. We find that the use of a relatively simple machine learning algorithm, combining phase-invariant orientation fields and image patches yield promising results. We then present a novel pixel-wise approach for centreline segmentation relying on phase information extracted after steering compact complex wavelets

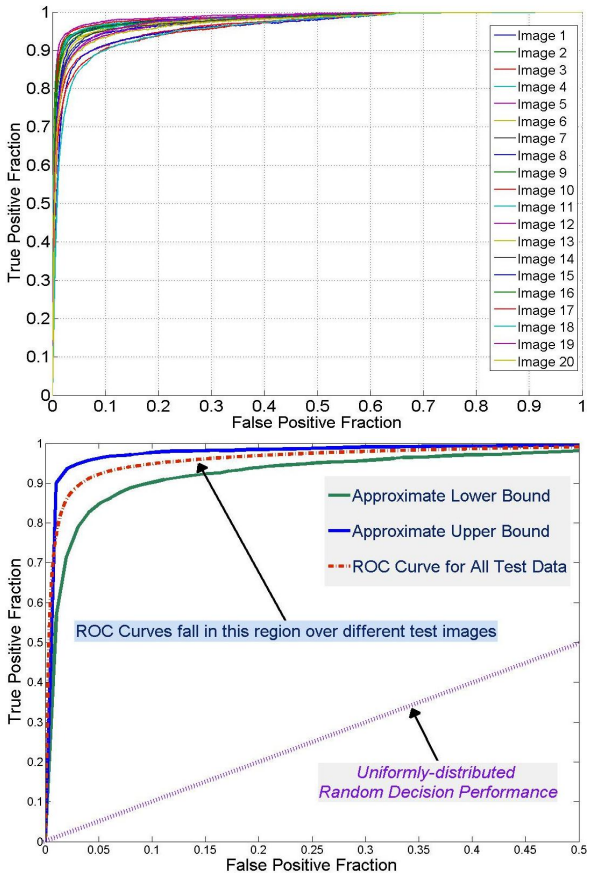

Fig. 5. *Top: The ROC curves for 20 test images using one neural network model; Bottom: The ROC curves for lower and upper bound, and for the entire test data.*

according to the orientation field; this can be used for evaluation of joint spatio-temporal registration accuracy and detection of microvascular occlusion possibly caused by microemboli [1]. A globally segmented vascular bed with locally extracted fine-resolution pathological microvasculatures allows clinicians to carry out longitudinal studies combining two existing imaging techniques, funduscopy and fluorescein angiography. This can eventually lead to a more personalized yet economical solution to monitor and treat patients with both current and historical medical records. Future development will include more extensive validation of the system on larger amounts of data, real-time performance evaluation and, in time, incorporation into a stand-alone system for clinical trials.

REFERENCES

[1] S. Cao, A. A. Bharath, K. Parker, J. Ng, J. Arnold, A. McGregor, and A. Hill, "Joint spatio-temporal registration and microvasculature segmentation of retinal angiogram sequences," in *2011 Annual International Conference of the IEEE Engineering in Medicine and Biology Society*, pp. 2618–2621.

[2] M. Niemeijer, J. J. Staal, B. van Ginneken, M. Loog, and M. D. Abramoff, "Comparative study of retinal vessel segmentation methods on a new publicly available database," *SPIE Medical Imaging*, vol. 5370, pp. 648–656, 2004.

[3] R. N. Weinreb and A. Harris, eds., *Ocular Blood Flow in Glaucoma*, ch. Clinical Measurement of Ocular Blood Flow, pp. 19–58. Kugler Publications, Amsterdam, The Netherlands, 2009.

[4] A. V. Stanton, B. Wasan, A. Cerutti, S. Ford, R. Marsh, P. P. Sever, S. A. Thom, and A. D. Hughes, "Vascular network changes in the retina with age and hypertension," *Journal of Hypertension*, vol. 13, no. 12, pp. 1724–1728, 1995.

[5] J. E. Grunwald, C. E. Riva, S. H. Sinclair, A. J. Brucker, and B. L. Petrig, "Laser doppler velocimetry study of retinal circulation in diabetes mellitus.," *Archives of Ophthalmology*, vol. 104, pp. 991–996, 1986.

[6] M. E. Langham, R. Farrell, T. Krakau, and D. Silver, "Ocular pulsatile blood flow, hypotensive drugs, and differential light sensitivity in glaucoma," in *Glaucoma Update IV* (G. K. Krieglstein, ed.), pp. 162–172, Berlin, Germany: Springer-Verlag, 1991.

[7] J. J. Staal, M. D. Abramoff, M. Niemeijer, M. A. Viergever, and B. van Ginneken, "Ridge based vessel segmentation in color images of the retina," *IEEE Transactions on Medical Imaging*, vol. 23, pp. 501–509, 2004.

[8] F. Zana and J. C. Klein, "A multimodal registration algorithm of eye fundus images using vessels detection and Hough transform," *IEEE Transactions on Medical Imaging*, vol. 18, no. 5, pp. 419–428, 1999.

[9] S. Chaudhuri, S. Chatterjee, N. Katz, M. Nelson, and M. Goldbaum, "Detection of blood vessels in retinal images using two-dimensional matched filters," *IEEE Transactions on Medical Imaging*, vol. 8, no. 3, pp. 263–269, 1989.

[10] A. Can, C. V. Stewart, B. Roysam, and H. L. Tanenbaum, "A feature based, robust, hierarchical algorithm for registering pairs of images of the curved human retina," *IEEE Transactions on Pattern Analysis and Machine Intelligence*, vol. 24, no. 3, pp. 347–364, 2002.

[11] M. E. Martinez-Perez, A. D. Hughes, A. V. Stanton, S. A. Thom, A. A. Bharath, and K. H. Parker, "Retinal blood vessel segmentation by means of scale-space analysis and region growing," in *Medical Image Computing and Computer-Assisted Intervention*, vol. 1679 of *Lecture Notes in Computer Science*, pp. 90–97, 1999.

[12] J. Ng, S. T. Clay, S. A. Barman, A. R. Fielder, M. J. Moseley, K. H. Parker, and C. Paterson, "Maximum liklihood estimatation of vessel parameters from scale space analysis," *Image Vision Computing*, vol. 28, no. 1, pp. 55–63, 2010.

[13] A. D. Hughes, "The clinical assessment of retinal microvascular structure and therapeutic implications," *Current Treatment Options in Cardiovascular Medicine*, vol. 9, pp. 236–241, 2007.

[14] A. A. Bharath, "Steerable filters from erlang functions," in *Proceedings of British Machine Vision Conference (BMVC)*, pp. 144–153, 1998.

[15] A. A. Bharath and J. Ng, "A steerable complex wavelet construction and its application to image denoising," *IEEE Transactions on Image Processing*, vol. 14, no. 7, pp. 948–959, 2005.

[16] J. Ng and A. A. Bharath, "Steering in scale space to optimally detect image structures," in *Proceedings of 8th European Conference on Computer Vision (ECCV)*, vol. 3021 of *LNCS*, pp. 482–494, 2004.

[17] Y. LeCun, L. Bottou, Y. Bengio, and P. Haffner, "Gradient-based learning applied to document recognition," *Proceedings of the IEEE*, vol. 86, no. 11, pp. 2278–2324, 1998.

[18] D. E. Rumelhart, G. E. Hinton, and R. J. Williams, "Learning internal representations by error propagation," in *Parallel Distributed Processing: Explorations in the Microstructure of Cognition* (D. E. Rumelhart and J. L. McClelland, eds.), ch. 8, Cambridge, MA and London, England: MIT Press, 1986.

[19] M. T. Hagan and M. B. Menhaj, "Training feedforward networks with the Marquardt algorithm," *IEEE Transactions on Neural Networks*, vol. 5, no. 6, pp. 989–993, 1994.

[20] S. Iftikhar, A. A. Bharath, A. R. Bond, A. I. Wagan, and P. D. Weinberg, "Segmentation of endothelial cell boundaries of rabbit aortic images using a machine learning approach," *International Journal of Biomedical Imaging*, 2011. Article ID 270247.

[21] M. Kass, A. Witkin, and D. Terzopoulus, "Snakes: Active contour models," *International Journal of Computer Vision*, pp. 321–331, 1988.

[22] R. O. Duda and P. E. Hart, "Use of the Hough transformation to detect lines and curves in pictures," *Communications of the ACM*, vol. 15, pp. 11–15, 1972.

[23] C. Steger, "An unbiased detector of curvilinear structures," *IEEE Transactions on Pattern Analysis and Machine Intelligence*, vol. 20, pp. 113–125, 1998.

[24] X. Jiang and D. Mojon, "Adaptive local thresholding by verification-based multithreshold probing with application to vessel detection in retinal images," *IEEE Transactions on Pattern Analysis and Machine Intelligence*, vol. 25, no. 1, pp. 131–137, 2003.

[25] B. Al-Diri, A. Hunter, and D. Steel, "An active contour model for segmenting and measuring retinal vessels," *IEEE Transactions on Medical Imaging*, vol. 28, no. 9, pp. 1488–97, 2009.